J. Fluid Mech. (2016), *vol.* 799, R2, doi:10.1017/jfm.2016.391

JFM RAPIDS
journals.cambridge.org/rapids

Linear instability analysis of low-*Re* incompressible flow over a long rectangular finite-span open cavity

Qiong Liu[1], **Francisco Gómez**[2] **and Vassilios Theofilis**[1,3,†]

[1]School of Aeronautics, Universidad Politécnica de Madrid, Madrid, Spain

[2]Department of Mechanical and Aerospace Engineering, Monash University, Victoria 3800, Australia

[3]School of Engineering, University of Liverpool, Browlow Hill, Liverpool L69 3GH, UK

(Received 13 March 2016; revised 25 May 2016; accepted 3 June 2016; first published online 21 June 2016)

TriGlobal linear instability analysis and direct numerical simulations have been performed to unravel the mechanisms ultimately responsible for transition of steady laminar flow over a long rectangular finite-span open cavity with dimensions $L:D:W = 6:1:2$ to unsteadiness. The steady laminar three-dimensional flow loses stability at $Re_{D,cr} \approx 1080$ as a consequence of linear amplification of a travelling eigenmode that is qualitatively analogous to the shear-layer mode known from analyses of flow in spanwise-periodic cavities, but has a three-dimensional structure which is strongly influenced by the cavity lateral walls. Differences in the eigenspectrum of the present and the spanwise homogeneous flow configuration are documented. Topological changes exerted on the steady laminar flow by linear amplification of the unstable shear-layer mode are reminiscent of observations in experiments at an order of magnitude higher Reynolds number.

Key words: instability, transition to turbulence

1. Introduction

A rectangular finite-span open cavity has been used extensively as a simplified model to understand flow in aircraft bays. Despite the apparent simplicity of the geometry, a multitude of physical phenomena arise, involving the shear layer emanating from the upstream cavity lip and its interaction with the downstream cavity corner, the boundary layers on the cavity walls, shock waves and expansion waves potentially existing at appropriate flow regimes, and acoustic waves generated at the cavity and propagating at long distances from it. From an engineering point of view, either of these aspects in isolation or their interaction can be seen at distinct

† Email address for correspondence: vassilis@aero.upm.es

flow regimes to affect noise emission from the cavity, structural integrity of landing gears, and safe release of stores.

Extensive research efforts over more than half a century have employed experimentation, numerical simulation and linear instability analysis in order to understand and control cavity flow physics. Table 1 summarizes a representative list of studies which have, at least partially, focused on flow instability in open cavities. While most practical applications use the full (three-dimensional, rectangular, finite-span) geometry, linear instability analyses of cavity flows to date have resorted to additional assumptions which make the resulting theoretical problem tractable. Most often spanwise flow homogeneity has been assumed, or flow over a two-dimensional cavity has been considered. The present work employs for the first time the theoretical TriGlobal instability analysis framework, which is appropriate for finite-span open cavities, as will be discussed shortly.

Research into open cavity flows commenced in the 1950s (Krishnamurty 1955; Roshko 1955) and has continued incessantly since. In an early significant contribution, Rossiter (1964) described a flow-acoustic resonance mechanism involving the interaction of the shear layer with the downstream cavity corner and derived a semi-empirical formula to predict the resonance frequencies, a work that has been extended by a number of authors since (e.g. Alvarez, Kerschen & Tumin 2004). Sarohia (1975, 1977) performed experiments and inviscid local linear instability analysis of laminar flow in a shallow axisymmetric cavity geometry and found that a large lateral motion of the shear layer occurs near the downstream lip. This three-dimensional motion results in a periodic shedding of vortices at a frequency of cavity oscillation different from those predicted by the Rossiter frequencies. In their classic experiment, Gharib & Roshko (1987) also employed the axisymmetric cavity geometry and described a flow behaviour, termed wake mode, which was found to be qualitatively distinct from that described by the quasi-parallel shear layer emanating from the upstream cavity lip. Rowley *et al.* (2002), in their two-dimensional direct numerical simulations (DNS), described both the shear-layer instabilities and those of the bluff-body-like wake mode, and associated the latter with absolute instability in the sense of Huerre & Monkewitz (1990), but did not employ the latter theory, applicable to one-dimensional base flow profiles, to describe the wake mode physics.

The linear instability analysis of Brés & Colonius (2008) employed modal BiGlobal theory to reveal a centrifugal instability mechanism associated with the main recirculation eddy inside the cavity, which was responsible for the loss of stability of two-dimensional cavity flows to three-dimensional instabilities. The frequency of this centrifugal instability, the characteristics of which were documented for a wide range of subsonic Mach numbers, was found to be one order of magnitude lower than that of the shear-layer mode. The periodic spanwise structure formation predicted in the analysis was found to be in good agreement with experimental observations in the same geometry (Faure *et al.* 2007, 2009). Meseguer *et al.* (2014) and Citro *et al.* (2015) have focused on the incompressible regime of spanwise-homogeneous flow and presented detailed linear BiGlobal instability analyses of the centrifugal linear instability mechanism; the latter work also discussed the means for theoretically founded control of this instability mechanism. Yamouni *et al.* (2013) revisited compressible flow over a rectangular open cavity and connected the global modes identified in their analysis with those predicted by the earlier cavity acoustics theories.

Experimentally, vortex shedding phenomena with a lateral motion downstream of the cavity were observed in a series of experiments performed in an axisymmetric cavity by Zhang & Naguib (2008) and a wall-bounded version of the same

https://doi.org/10.1017/jfm.2016.391 Published online by Cambridge University Press

References	Geometry	M	L/D	L/W	Re	θ_0
Sarohia (1977)	*ax*	0.015	0–50	—	2×10^4–10^5	—
Gharib & Roshko (1987)	*ax*	0.00015	0.678 0.985 1.081	—	1.2×10^4	0.041
Rowley, Colonuis & Basu (2002)	2d	0.2–0.8	1 2 3 4 5 6 8	—	750–3748.3	0.0162–0.0985
Sun *et al.* (2014)	2d	0.1–1.6	2	—	238–3802	0.0379
		0.1–1.2	6		132–1214	
Özsoy *et al.* (2005)	*sh*	0–0.0582	4	3.75	4000	0.035
					9000	0.028
					13000	0.025
Faure *et al.* (2007)	*sh*	0.1–1.6	2	0.333	275–5335	—
Brés & Colonius (2008)	*sh*	0.1–0.8	1 2 4	0.2 0.25 2 3.2	755–6960	0.0033–0.0571
Faure *et al.* (2009)	*sh*	0.01	0.25–2.5	0.125–4.8	1150–36800	—
De Vicente *et al.* (2014)	*sh*	—	2	0.796–6.369	1100–2400	0.0363–0.0392
Meseguer *et al.* (2014)	*sh*	—	1.0, 1.1, 1.2, 1.3 1.4 1.5 2 3	0.0455–∞	800–4600	0.1157–0.3
Yamouni, Sipp & Jacquin (2013)	*sh*	0.04–0.9	1 2	—	7500	0.0043–0.0292
Citro, Brandt & Luchini (2015)	*sh*	—	1	2.134	1370	0.0113
				3.503	4140	0.0065

TABLE 1. Continued on next page.

https://doi.org/10.1017/jfm.2016.391 Published online by Cambridge University Press

References	Geometry	M	L/D	L/W	Re	θ_0
Douay, Pastur & Lusseyran (2016)	*sh*	—	1.2–2	0.1–0.166	1600–3200	$O(10^{-3})$
Forestier, Jacquin & Geffroy (2003)	3d	0.8	0.42	0.42	2.048×10^6	0.0054
Yao, Cooper & Raghunathan (2004)	3d	—	1	0.333	3000 10000	0.008 0.015
						0.013 0.028
			2		3000	0.013
			4		3000 10000	0.013
Larchevêque *et al.* (2004)	3d	0.85	5	5	1.4×10^6	—
Ashcroft & Zhang (2005)	3d	~ 0.1	2.0	0.111	1.1×10^5	—
			3.0	0.167	1.3×10^5	
			4.0	0.222	1.4×10^5	
Larchevêque, Sagaut & Labbé (2007)	3d	0.8	2	0.42	4.3×10^5	—
Zhang & Naguib (2008, 2011)	3d	—	3.4	0 0.479	4067	0.169
				1.417 0.971	12200	0.252
Crook, Lau & Kelso (2013)	3d	—	6	3	7.167×10^3	0.01
					5.667×10^4	0.011
Zhang *et al.* (2015)	3d	0.33 0.43 0.53	6	1.56	4×10^5	4.46×10^{-4}
		0.63 0.73				5.09×10^{-4}
George *et al.* (2015)	3d	1.4	6	3	4×10^6	3.187×10^{-4}

TABLE 1 (cntd). A representative list of works describing linear instabilities in rectangular open cavity flows, using linear and nonlinear instability analysis, simulations and experiments; *ax* denotes axisymmetric geometry and *sh* indicates three-dimensional cavity in which spanwise-homogeneous flow is assumed. *Re* is based on *D*.

geometry by Zhang & Naguib (2011). The detected frequencies were consistent with those found by Sarohia (1977) but different from those predicted by the Rossiter theory. In this context, the numerical experiments of Yao *et al.* (2004) on unsteady incompressible three-dimensional cavity flow indicated that, at sufficiently high Reynolds number, both three-dimensional centrifugal modes and shear-layer modes may co-exist and interact. In an analogous vein, the experimental work of George *et al.* (2015) employed stereo particle image velocimetry (PIV) measurements to show that the effect of the sidewalls in the cavity flow is also relevant; their experiments revealed that the frequency of the dominant Rossiter mode varies when comparing different spanwise aspect ratio cavities, with and without lateral walls. The experiments of Ashcroft & Zhang (2005) employed PIV measurements to analyse turbulent flow over a large-width cavity and documented the presence of shear-layer instabilities in turbulent flow. Özsoy *et al.* (2005) also experimented with turbulent flow and described vortex motions inside the cavity. Crook, Kelso & Drobik (2007), Crook *et al.* (2013) performed experiments with the full three-dimensional geometry and postulated that a single vortex located near the cavity centreline was responsible for asymmetries observed in the cavity flow. The observed asymmetry in the time-mean flow was due to the asymmetries in the instantaneous flow field, which switched between two extremes at low frequency. These authors associated this motion with centrifugal instability, but with a more three-dimensional complex pattern. De Vicente *et al.* (2014) further described the centrifugal instability in a combined theoretical and experimental work, while very recently Douay *et al.* (2016) have performed experimental work exclusively dedicated to the description of this mechanism. Large-scale simulations have employed DNS to fully resolve the two-dimensional (Sun *et al.* 2014) or three-dimensional spanwise-homogeneous (Zhang *et al.* 2015) and finite-span cavity (Yao *et al.* 2004), as well as large eddy simulation for the latter geometry (Forestier *et al.* 2003; Larchevêque *et al.* 2004, 2007; Nayyar, Barakos & Badcock 2007). Useful as they may be in the identification of physical mechanisms, large-scale simulations are hardly appropriate for parametric studies of the dependence of instability characteristics on geometric or flow parameters. A full discussion of the intense efforts to control cavity flow, also by exploiting the hitherto understood linear instability mechanisms, may be found in the excellent reviews of Cattafesta *et al.* (2008) and the related work on actuators of Cattafesta & Sheplak (2011).

Despite this intense activity, to date the question of the origins of laminar–turbulent transition in the cavity model closest mimicking the desired application, namely a three-dimensional, rectangular, finite-span open cavity, is still open. Evidence does exist in the literature to suggest that the lateral walls have a profound influence on the flow features, and hence on their instability modes. Motivated by the fact that all linear instability work on open cavities has been performed either in a local framework, or assuming flow homogeneity along the span, the present work employs for the first time the TriGlobal modal analysis framework (Theofilis 2003) appropriate for rectangular finite-span open cavities.

Section 2 defines the geometric and flow parameters considered. The cavity geometry employed by Crook *et al.* (2013) and others in their experiments is chosen in order to facilitate comparisons, albeit qualitative on account of the lower Reynolds numbers at which instabilities have been identified; flow topology is used to relate the two sets of results. Three-dimensional DNS is performed in § 3.1 in order to obtain the base flows to be analysed, either by time-marching the full equations of motion until convergence in the subcritical regime, or by employing a selective frequency

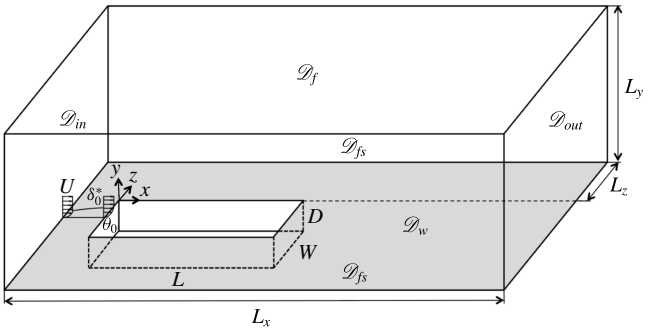

FIGURE 1. Configuration of the three-dimensional open cavity.

Re	900	950	1000	1050	1100
D/θ_0	31.948	32.823	33.676	34.507	35.319
δ_0^*	0.081	0.079	0.077	0.075	0.073
$Re_{\delta_0^*}$	73.007	75.008	76.957	78.857	80.731

TABLE 2. Summary of the flow parameters considered in the analysis. Subscript 0 refers to conditions at the upstream edge of the cavity.

damping (SFD) technique in order to obtain steady unstable three-dimensional flows beyond the first bifurcation. Linear instability analysis results are presented in § 3.2 and their relation to those obtained by assuming spanwise-homogeneous flow is discussed in § 3.3. Topological reconstruction of the main flow features is used to provide a qualitative comparison of the present theoretical results with the available experimental results. A short discussion in § 4 closes the present contribution.

2. Problem formulation

A sketch of the rectangular finite-span open cavity flow configuration walls is shown in figure 1. The cavity geometry is characterized by a length L to depth D to width W ratios of $L:W:D = 6:2:1$. A Cartesian coordinate system with (x, y, z) the streamwise, wall-normal and spanwise direction, respectively, is considered and the origin $(0, 0, 0)$ is fixed at the upstream left corner of the cavity. The velocity vector $\boldsymbol{u}(x, y, z, t)$ comprises the corresponding Cartesian components $(u, v, w)^{\mathrm{T}}$, all of which are inhomogeneous functions of the three spatial coordinates and time. The length, height and width of the computational domain are denoted by L_x, L_y and L_z, respectively. The domain boundaries $\mathscr{D}_{in}$, $\mathscr{D}_w$, $\mathscr{D}_f$, $\mathscr{D}_{out}$ and $\mathscr{D}_{fs}$ denote inflow, wall, far-field, outflow and side wall boundaries, respectively. The flow is governed by three-dimensional incompressible Navier–Stokes and continuity equations, and the Reynolds number is based on the cavity depth $Re = UD/\nu$, where $U = 1$ is the streamwise velocity in the far field and ν is the kinematic viscosity. A laminar Blasius boundary layer is imposed at the inflow boundary and the flow parameters are chosen such that no boundary layer instabilities develop prior to the upstream cavity lip. The parameter ratio of cavity length to initial boundary layer momentum thickness, L/θ, boundary layer displacement thickness δ^* and displacement thickness Reynolds number $Re_{\delta^*} = U\delta^*/\nu$ are fixed at the values listed in table 2.

Direct numerical simulations are performed with the spectral element code Nek5000 (Fischer & Ronquist 1994). The boundary conditions used to obtain the solutions analysed are homogeneous Dirichlet on the wall boundary $\mathscr{D}_w$, $(u, v, w) = (u_B, v_B, 0)$ at the inflow boundary $\mathscr{D}_{in}$, $(u, \partial v/\partial n, w) = (U, 0, 0)$ on the far-field boundary $\mathscr{D}_f$, $(\partial u/\partial n, \partial v/\partial n, w) = \boldsymbol{0}$ on the lateral boundaries $\mathscr{D}_{fs}$ and $(p - (1/Re)\boldsymbol{\nabla u}) \cdot \boldsymbol{n} = 0$ on the outflow boundary $\mathscr{D}_{out}$. The subscript B denotes Blasius boundary layer profile. The computational domain above the cavity is initialized with an incompressible Blasius boundary layer profile, while the flow inside the cavity is initially taken to be at rest.

The linear instability of the flow to small-amplitude perturbations has been analysed using a modal TriGlobal approach (Theofilis 2003, 2011), following which flow is decomposed into a steady base flow $\bar{\boldsymbol{u}}$ and a small amplitude time-varying three-dimensional perturbation $\hat{\boldsymbol{u}}$ according to

$$\boldsymbol{u}(x, y, z, t) = \bar{\boldsymbol{u}}(x, y, z) + \epsilon \hat{\boldsymbol{u}}(x, y, z) \mathrm{e}^{\lambda t} + \text{c.c.} \tag{2.1}$$

Here $\lambda = \lambda_r + \mathrm{i}\lambda_i$, where λ_r denotes the temporal amplification/damping rate of the perturbations, λ_i is the perturbation frequency, c.c. denotes the complex conjugate and $\epsilon \ll 1$. Introduction of this decomposition into the equations of motion and linearization yields the linearized Navier–Stokes equations (LNSE), which can be recast as the three-dimensional eigenvalue problem

$$\boldsymbol{A}\hat{\boldsymbol{u}} = \lambda \hat{\boldsymbol{u}}, \tag{2.2}$$

at $O(\epsilon)$, in which the operator $\boldsymbol{A}$ is an abbreviation for the Jacobian. The boundary conditions closing (2.2) are homogeneous Dirichlet on all perturbation velocity components on $\mathscr{D}_{in}$ and $\mathscr{D}_w$ alongside $(\hat{u}, \partial \hat{v}/\partial n, \hat{w}) = \boldsymbol{0}$ on $\mathscr{D}_f$, $(\partial \hat{u}/\partial n, \partial \hat{v}/\partial n, \hat{w}) = \boldsymbol{0}$ on $\mathscr{D}_{fs}$ and $(\hat{p} - (1/Re)\boldsymbol{\nabla}\hat{\boldsymbol{u}}) \cdot \boldsymbol{n} = 0$ on $\mathscr{D}_{out}$. The eigenvalue problem (2.2) is solved for the recovery of λ and $\hat{\boldsymbol{u}}$ using the time-stepping methods provided in Nek5000 (Peplinski *et al.* 2014).

For comparison purposes with the more commonly employed BiGlobal linear modal analysis framework for the analysis of open cavity flow, the related Ansatz is also presented here. In the case of spanwise homogeneous base flow, linear global modal perturbations satisfy the expansion

$$\boldsymbol{u}(x, y, z, t) = \bar{\boldsymbol{u}}(x, y) + \epsilon \hat{\boldsymbol{u}_{2d}}(x, y) \mathrm{e}^{\mathrm{i}(\beta z + \lambda_i t)} \mathrm{e}^{\lambda_r t} + \text{c.c.} \tag{2.3}$$

The eigenvalue problem resulting from substituting (2.3) into the LNSE has also been solved here and results will be discussed in the next section. In the present work the BiGlobal eigenvalue problem is also solved by a time-stepping approach, in a three-dimensional domain in which the base flow is uniform along z. Periodic boundary conditions are imposed along the spanwise spatial direction, which, for a given wavenumber of interest, β, is taken to have a length of $L_z = 2\pi/\beta$. Consequently, modes corresponding to $\beta = 0$ or multiples of the imposed β may appear in the results.

3. Results

3.1. *Base flow*

At the set of flow parameters chosen our first concern has been to establish independence of the steady base flows analysed from the choice of size of computational domain and polynomial order used to resolve the base state and

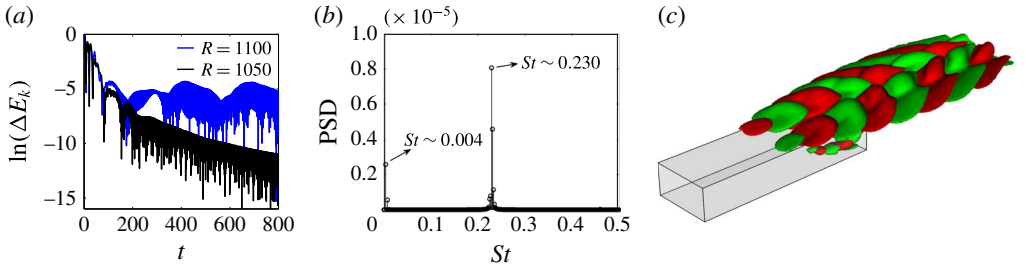

FIGURE 2. (*a*) Convergence history of $\ln(\Delta E_k)$ against time. (*b*) Power spectral density of $\ln(\Delta E_k)$ at $Re = 1100$. (*c*) Spanwise fluctuation velocity component.

its gradients. As regards the extent of the domain, it was found that $L_x = 13$, $L_y = 5$ and $L_z = 4$ are the lowest values in the three spatial directions which ensure that the base state obtained in the cavity is independent of the lateral, top and downstream boundary locations.

Once the minimum domain size has been established, the `genbox` utility of nek5000 has been used to create a mesh comprising a total of 9696 elements. This has been kept constant in the subsequent computations, while the polynomial order has been varied between $p = 5$, 7 and 9, until convergence of the vorticity components at randomly chosen locations within the domain was obtained; details may be found in Liu (2016). In order to maintain the computing cost at a minimum while convergence is ensured, $p = 7$ has been selected for the computations that follow.

Preliminary work on the same geometry and flow conditions has identified the critical Reynolds number at $Re \approx 1100$ (Liu, Gómez & Theofilis 2015). Below this value direct DNS have been performed until convergence to a steady state has been reached, while above this value the selective frequency damping (SFD) algorithm (Åkervik *et al.* 2006), as implemented in the nek5000 code, has been used to obtain steady unstable three-dimensional flows that will subsequently be analysed. It should be noted in this context that the critical Reynolds number of an $L:D = 6:1$ cavity, in which spanwise-homogeneous flow is considered, is $Re \approx 790$ (Sun *et al.* 2014), as extrapolated from the results of these authors at the limit Mach number $M \to 0$, a point which will be discussed further in what follows.

Figure 2(*a*) presents DNS results at $Re = 1050$ and 1100. Shown is the perturbation energy $\Delta E_k = |E_k(t) - \bar{E}_k|$, where $E_k = \int_\Omega \boldsymbol{u} \cdot \boldsymbol{u}\, \mathrm{d}\Omega$ and $\bar{E}_k$ is the solution at convergence. At $Re = 1050$, a linearly decaying signal is observed, which results in a steady state being obtained at convergence. By contrast, at $Re = 1100$ the flow attains a saturated state in which both a low-frequency and a high-frequency oscillation are visible. Fourier transforming the signal, two frequencies may be identified, $St = \lambda_i D/U \approx 0.004$ and $St \approx 0.23$, as shown in figure 2(*b*). Isosurfaces $\Delta w = \pm 0.008$ of the spanwise component of the fluctuating velocity vector are presented in figure 2(*c*) and will be discussed in what follows.

3.2. *Linear instability analysis*

Results of TriGlobal linear modal instability analysis performed for the stationary base flows at $Re = 900$, 950, 1000 and 1050, and the steady unstable base flow obtained with the SFD algorithm, using filter width $\Delta = 2$ and force control parameter $\chi = 0.8$, at $Re = 1100$ are shown in table 3. At $Re = 900$ and 950, the leading global mode

https://doi.org/10.1017/jfm.2016.391 Published online by Cambridge University Press

			$\lambda_r \pm \mathrm{i}\lambda_i$		
Mode	$Re = 900$	$Re = 950$	$Re = 1000$	$Re = 1050$	$Re = 1100$
CS	$-0.0136 \pm \mathrm{i}0.0000$	$-0.0132 \pm \mathrm{i}0.0000$	$-0.0128 \pm \mathrm{i}0.0000$	$-0.0124 \pm \mathrm{i}0.0000$	$-0.0127 \pm \mathrm{i}0.000$
CT	$-0.0198 \pm \mathrm{i}0.0340$	$-0.0181 \pm \mathrm{i}0.0344$	$-0.0163 \pm \mathrm{i}0.0345$	$-0.0149 \pm \mathrm{i}0.0347$	$-0.0132 \pm \mathrm{i}0.035$
ST	—	—	$-0.0260 \pm \mathrm{i}1.4463$	$-0.0100 \pm \mathrm{i}1.4543$	$+0.0077 \pm \mathrm{i}1.462$

TABLE 3. The leading eigenvalues of the centrifugal steady (CS), centrifugal travelling (CT) and shear-layer travelling (ST) mode in the Reynolds number range examined.

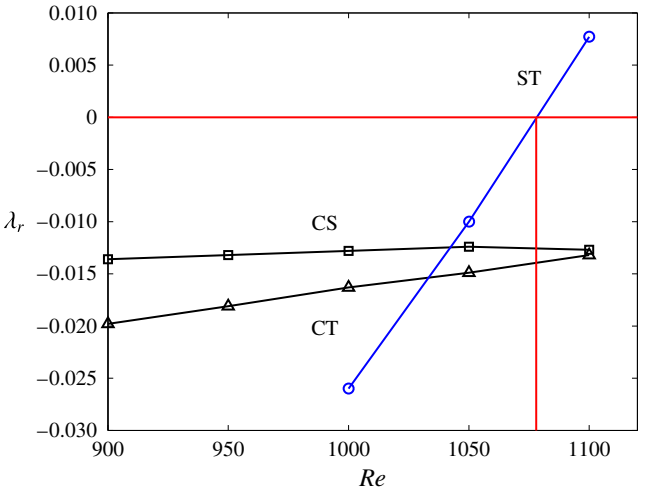

FIGURE 3. Dependence of λ_r on Re for the cavity modes ST, CS and CT.

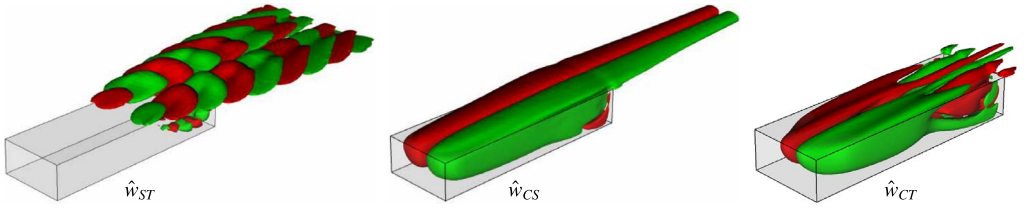

FIGURE 4. Spanwise amplitude functions of the leading cavity eigenmodes at $Re = 1050$.

is stable and stationary, having a spatial structure reminiscent of the centrifugal instability known from analyses of the spanwise-homogeneous cavity, as has been discussed by Brés & Colonius (2008) and earlier related work (e.g. Barkley, Gomez & Henderson 2002). This mode is referred to as the centrifugal stationary (CS) eigenmode. Additional modes having low frequencies and analogous spatial structure of the eigenfunctions, but being stronger damped, have also been recovered. The next of them is referred to as the centrifugal travelling (CT) mode. When the Reynolds number is increased to $Re = 1000$, the leading mode is still the CS perturbation, however, besides this and the CT mode, a new global mode appears in the subset of the eigenspectrum recovered, having a relatively higher frequency than the CT mode, $St \approx 0.23$. Owing to the spatial structure of its amplitude function, this mode is termed the shear-layer travelling (ST) eigenmode. When the flow Reynolds number is further increased to $Re = 1050$, the ST mode becomes the leading eigenvalue, its λ_r exceeding the damping rates of both of the CT and CS instabilities, and finally becoming unstable, leading flow to a modally unstable state and ultimately to laminar–turbulent transition. The critical Reynolds number is obtained using linear interpolation of the damping/growth rate results of the ST mode either side of the $\lambda_r = 0$ axis, as shown in figure 3. The zero crossing of the $\lambda_{r,ST}$ eigenvalue in this open cavity configuration is estimated to occur at $Re_{cr} \approx 1080$.

The spatial structure of the amplitude functions of global modes ST, CS and CT at $Re = 1050$ is illustrated in figure 4. Eigenfunctions are normalized with their

respective max $|\hat{u}|$ values and isosurfaces $\hat{u} = \pm 0.1$, $\hat{v}$, $\hat{w} = \pm 0.05$ are shown. Visual inspection of the amplitude functions reveals that the velocity field of the ST mode corresponds to three-dimensional shedding oscillations near the downstream corner of the cavity, which exhibit typical shear-layer mode characteristics. However, the mode structure is different from an idealized spanwise-homogeneous Kelvin–Helmholtz perturbation, as it has a more complex spatial structure owing to the proximity of the lateral walls. Such behaviour can be interpreted as being qualitatively related to that found in earlier experimental work (Sarohia 1977; Zhang & Naguib 2008), according to which no vortex structures are to be observed in the neighbourhood of the leading edge of the cavity, while self-sustained oscillations are seen near the downstream cavity corner, caused by convective waves accompanied by a large lateral flapping motion. The present results identify the origin of the latter motion in the existence of the spanwise perturbation velocity $\hat{w}_{ST}$ of the ST mode.

The amplitude functions of the CS and CT modes, also shown in figure 4, are three-dimensional structures mainly confined inside the cavity, which peak in the neighbourhood of the three-dimensional base flow recirculation region of the cavity (Liu 2016). The characteristic structure of the $\hat{w}$ perturbation component of both of these modes is reminiscent of the pattern found in the spanwise-homogeneous cavity (Brés & Colonius 2008), although in the latter case alternating maxima and minima of the spanwise perturbation velocity are repeated, in line with the imposed periodicity wavenumber. By contrast, in the present lateral-wall-bounded cavity, only one such structure, symmetric about the plane $z = 1$, can be seen in the $\hat{w}$ amplitude functions of both of the CS and CT eigenmodes.

Returning to the ST mode, additional evidence regarding its potential relevance to transition in the open cavity at higher Reynolds numbers is provided by the fact that its frequency is found to remain approximately constant in the instability analysis at $Re = 1000$ and 1050, and is practically identical to the highest of the frequencies extracted by post-processing the DNS signal of nonlinearly saturated flow at $Re = 1100$, shown in figure 2(*b*). In other words, the dynamics of flow at $Re = 1100$ appears to be dominated by the ST mode, a conjecture corroborated by the comparison of the spatial structure of the spanwise velocity component obtained in the DNS at $Re = 1100$, shown in figure 2(*c*) with the amplitude function of the $\hat{w}_{ST}$ component of the perturbation velocity at $Re = 1050$, shown in figure 4; the respective three-dimensional functions are practically indistinguishable.

Next, an attempt is made to relate the present finding of linear instability of the ST mode with the result of earlier experimental work of Crook *et al.* (2007) in which the exact same geometry has been utilized, albeit at an order-of-magnitude higher Reynolds number value. Topological bifurcations (Délery 2013) exerted by the ST, CS and CT modes on the underlying steady three-dimensional base flow have been examined by Liu (2016), using a methodology analogous to that employed in earlier analyses of three-dimensional separated flows (Theofilis, Hein & Dallmann 2000; Rodríguez & Theofilis 2011; Le Clainche *et al.* 2015). The near-wall-streamline pattern of a composite three-dimensional field is computed, in which the base state and its leading eigenmode are superposed linearly at an arbitrary but small amplitude parameter ϵ.

Figure 5(*a*) shows the wall-streamline result for the ST mode at an amplitude $\epsilon = 0.1$, while in (*b*) the experimental result of Crook *et al.* (2007) is presented. Compared with their counterparts constructed using the CS and CT modes (Liu 2016), the wall-streamline pattern of the composite field corresponding to the ST mode is that which closest resembles the streamline curvature pattern seen in the experiment.

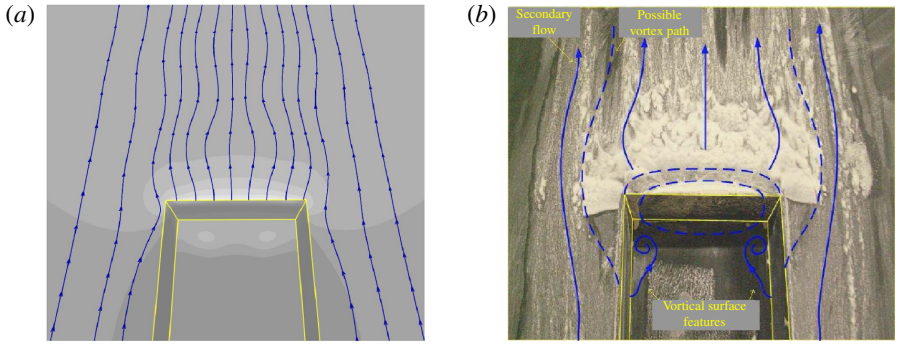

FIGURE 5. (*a*) Wall streamlines of the composite field constructed with the ST mode at $Re = 1050$. (*b*) Streamlines depicted in the experiments of Crook *et al.* (2007) at $Re \approx 1.66 \times 10^4$ (reproduced with permission).

The two vortices predicted experimentally to exist near the downstream corners of the cavity (cf. Crook *et al.* 2013) can also be identified as greyscale pressure minimum contours in the theoretical results. At the higher Reynolds number of the experiment, additional eigenmodes may have become unstable and will modify the theoretical wall-streamline pattern, such that the qualitative agreement presented may still be fortuitous. Nevertheless, this result motivates renewed combined theoretical and experimental efforts at the exact same parameters, in order to further elucidate the laminar–turbulent transition scenario in this flow.

3.3. *Instability in spanwise-homogeneous cavities*

Instability analysis of flow over spanwise-homogeneous cavities has been performed in order to enable quantitative comparisons with the results of the lateral-wall-bounded open cavity discussed in the previous sections. Two spanwise-homogeneous configurations have been chosen, the square cavity discussed by Citro *et al.* (2015) at $Re = 4140$, $\beta = 22$ with which comparisons of the leading eigenmodes have been performed, as well as a cavity with aspect ratio $L:D = 6:1$ (Sun *et al.* 2014) in which analysis has been performed at $Re = 1000$, $\beta = \pi$. The conditions examined in both configurations correspond to linearly unstable flow; the eigenvalue spectrum is presented in the former work, while a critical Reynolds number $502 \leqslant Re \leqslant 634$ has been reported in the latter at Mach number $M = 0.1$. In the present analysis, three-dimensional DNS making use of the SFD algorithm is used to obtain the basic states in both configurations.

The leading members of the eigenvalue spectrum obtained in the first configuration were found to be in good agreement with the results reproduced graphically from Citro *et al.* (2015) and shown alongside our results for both open cavity configurations in table 4 (Liu 2016). Of particular interest in the present context is the second configuration, in which the spanwise periodicity length, $\Lambda = 2\pi/\beta = 2$, is identical to the width $W = 2$ of the wall-bounded cavity analysed in the earlier sections. Comparing the results of table 3 at $Re = 1000$ and those of table 4 for the $L:D = 6:1$ cavity, it is seen that the leading eigenvalues of the former cavity, pertinent to the (linearly stable) lateral-wall-bounded flow and those of the (linearly unstable) spanwise-homogeneous flow in the $L:D = 6:1$ cavity with periodicity length $\Lambda = 2$, bear no resemblance to each other. Besides the opposite signs of

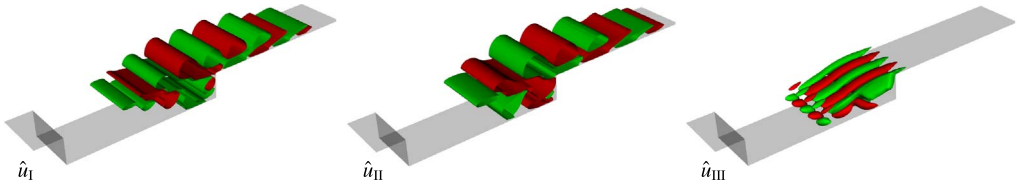

FIGURE 6. Streamwise perturbation velocities of the leading three modes of a $L:D = 6:1$ spanwise-homogeneous cavity at $Re = 1000$ whose eigenvalues are shown in table 4.

	$L:D = 1:1$				$L:D = 6:1$		
	Citro *et al.* (2015)		Present results				
Mode	λ_r	λ_i	λ_r	λ_i	Mode	λ_r	λ_i
I	0.233	0	0.2380	0	I	0.0850	$\pm$1.0537
II	0.218	$\pm$0.260	0.2243	$\pm$0.3005	II	0.0798	$\pm$1.5313
III	0.176	$\pm$0.567	0.1811	$\pm$0.6036	III	0.0320	$\pm$0.2427
IV	0.113	$\pm$0.886	0.1176	$\pm$0.9134	—	—	—

TABLE 4. Leading eigenvalues in the spanwise-periodic open cavity $L:D = 1:1$ at $Re = 4140$, $\beta = 22$ and in the $L:D = 6:1$ cavity at $Re = 1000$, $\beta = \pi$.

the amplification rates λ_r of all three modes, none of the frequencies, λ_i, in either set of results coincides with any mode pertaining to the other configuration. The stationary perturbation in the lateral-wall-bounded flow is altogether absent in the spanwise-homogeneous case. On the other hand, the fact that the frequencies of the travelling modes in the two configurations are of the same order of magnitude may be considered as being fortuitous.

The last statement is strengthened by reference to the amplitude functions obtained in BiGlobal linear modal analysis of the spanwise homogeneous open cavity flow. The streamwise perturbation velocity components of the three modes pertinent to the $L:D = 6:1$ cavity shown in table 4 are presented in figure 6 as isosurfaces $\hat{u} = \pm 0.2$, after being scaled with their respective $\max(\hat{u})$ values. The first two modes are seen to correspond to $\beta = 0$ and be independent of the z-spatial direction, a fact that is certainly not true in any of the corresponding eigenfunctions shown in figure 4. Indeed, Modes I and II of the spanwise-homogeneous base flow are typical Rossiter modes further discussed by Liu (2016), while the well-defined spanwise-periodic structure of Mode III, known from earlier analyses and experiments to be related to centrifugal instability, is also different from the spatial structure of the amplitude functions of the CS or CT modes, in which the lateral-wall effect are evident.

4. Discussion and conclusions

Incompressible flow over a three-dimensional rectangular finite-span open cavity with $L:W:D = 6:2:1$ has been analysed with respect to its linear instability from subcritical to supercritical conditions. TriGlobal linear analysis has been employed for the first time to this class of flows, and the critical Reynolds number was determined to be $Re_{cr} \sim 1080$. The mode responsible for the first bifurcation from steady to unsteady flow that may lead to laminar–turbulent flow transition at higher Reynolds numbers is akin to the well-known shear-layer instability, although the lateral walls

have a strong effect on the amplitude function. Direct numerical simulations at supercritical Reynolds numbers confirmed the existence and predominance of the shear-layer mode. Linear amplification of the leading shear-layer eigenmode gives rise to large lateral motions near the downstream cavity wall, while wall-streamline patterns corresponding to the linear superposition of the base flow and this mode are reminiscent of experimental results at one order of magnitude higher Reynolds number. Additional eigenmodes have been discovered, arising from centrifugal instability associated with the three-dimensional laminar separation bubble forming inside the cavity. The centrifugal instabilities are less damped than the shear-layer mode at lower Reynolds numbers, but have not become unstable in the Reynolds number range examined presently. Results of the present analysis have been compared with those pertinent to the well-understood spanwise homogeneous open cavity configuration having the same length-to-depth ratio. Strong differences were documented both in the critical Reynolds number values of the two configurations, as well as in the frequencies and spatial structure of the amplitude functions of all modes identified in the respective analyses, a result which underlines the need to employ modal TriGlobal linear stability theory in order to understand the origins of laminar–turbulent flow transition in three-dimensional open cavity geometries.

Acknowledgements

Q.L. gratefully acknowledges a research scholarship of the Chinese Scholarship Council and additional support from Nu-Modelling SL, in the framework of Grant FA9550-13-1-0059 of the Air Force Office of Scientific Research, Air Force Material Command, USAF and Subaward A12494 of Rensselaer Polytechnic Institute. The US Government is authorized to reproduce and distribute reprints for Governmental purpose not withstanding any copyright notation thereon.

References

Åkervik, E., Brandt, L., Henningson, D. S. & Hœpffner, J. 2006 Steady solutions of the Navier–Stokes equations by selective frequency damping. *Phys. Fluids* **18**, 068102,1–4.

Alvarez, J., Kerschen, E. J. & Tumin, A. 2004 A theoretical model for cavity acoustic resonance in subsonic flow. *AIAA Paper* 2004-2845.

Ashcroft, G. & Zhang, X. 2005 Vortical structures over rectangular cavities at low speed. *Phys. Fluids* **17**, 015104,1–8.

Barkley, D., Gomez, M. G. & Henderson, R. D. 2002 Three-dimensional instability in flow over a backward-facing step. *J. Fluid Mech.* **473**, 167–190.

Brés, G. A. & Colonius, T. 2008 Three dimensional instabilities in compressible flow over open cavity. *J. Fluid Mech.* **599**, 309–339.

Cattafesta, L. N. & Sheplak, M. 2011 Actuators for active flow control. *Annu. Rev. Fluid Mech.* **43**, 247–272.

Cattafesta, L. N., Song, Q., William, D. R., Rowley, C. W. & Alvi, F. S. 2008 Active control of flow-induced cavity oscillations. *Prog. Aerosp. Sci.* **44**, 479–502.

Citro, V. F. G., Brandt, L. & Luchini, P. 2015 Linear three-dimensional global and asymptotic stability analysis of incompressible open cavity flow. *J. Fluid Mech.* **768**, 113–140.

Crook, S., Kelso, R. & Drobik, J. 2007 Aeroacoustics of aircraft cavities. In *16th Australasian Fluid Mechanics Conference (AFMC)* (ed. P. Jacobs, T. Mclntyre & M. Cleary), pp. 429–435. School of Engineering, The University of Queensland.

Crook, S. D., Lau, T. C. W. & Kelso, R. M. 2013 Three-dimensional flow within shallow, narrow cavities. *J. Fluid Mech.* **735**, 587–612.

Délery, J. 2013 *Three-Dimensional Separated Flow Topology*. Wiley.

DE VICENTE, J., BASLEY, J., MESEGUER, F., SORIA, J. & THEOFILIS, V. 2014 Three dimensional instabilities over a rectangular open cavity: from linear stability analysis to experimentation. *J. Fluid Mech.* **748**, 189–220.

DOUAY, C. L., PASTUR, L. R. & LUSSEYRAN, F. 2016 Centrifugal instabilities in an experimental open cavity flow. *J. Fluid Mech.* **788**, 670–694.

FAURE, T. M., ADRIANOS, P., LUSSEYRAN, F. & PASTUR, L. 2007 Visualizations of the flow inside an open cavity at medium range Reynolds numbers. *Exp. Fluids* **42**, 169–184.

FAURE, T. M., PASTUR, L. R., LUSSEYRAN, F., FRAIGNEAU, Y. & BISCH, D. 2009 Three-dimensional centrifugal instabilities development inside a parallelepipedic open cavity of various shapes. *Exp. Fluids* **47** (3), 395–410.

FISCHER, P. F. & RONQUIST, E. M. 1994 Spectral element methods for large scale parallel Navier–Stokes calculations. *Comput. Meth. Appl. Mech. Engng* **116**, 69–76.

FORESTIER, N., JACQUIN, L. & GEFFROY, P. 2003 The mixing layer over a deep cavity at high-subsonic speed. *J. Fluid Mech.* **475**, 101–145.

GEORGE, B., UKEILEY, L., CATTAFESTA, L. N. & TAIRA, K. 2015 Control of three-dimensional cavity flow using leading-edge solt slowing. *AIAA Paper* 2015-1059.

GHARIB, M. & ROSHKO, A. 1987 The effect of flow oscillations on cavity drag. *J. Fluid Mech.* **177**, 501–530.

HUERRE, P. & MONKEWITZ, P. A. 1990 Local and global instabilities in spatially developing flows. *Annu. Rev. Fluid Mech.* **22**, 473–537.

KRISHNAMURTY, K. 1955 Acoustic radiation from two dimensional rectangular coutouts in aerodynamic surfaces. *NACA TN* 3487.

LARCHEVÊQUE, L., SAGAUT, P. & LABBÉ, O. 2007 Large-eddy simulation of a subsonic cavity flow including asymmetric three-dimensional effects. *J. Fluid Mech.* **577**, 105–126.

LARCHEVÊQUE, L., SAGAUT, P., LÊ, T. H. & COMTE, P. 2004 Large-eddy simulation of compressible flow in a three-dimensional open cavity at high Reynolds number. *J. Fluid Mech.* **516**, 265–301.

LE CLAINCHE, S., LI, J. I., THEOFILIS, V. & SORIA, J. 2015 Flow around a hemisphere-cylinder at high angle of attack and low Reynolds number. *Aerosp. Sci. Technol.* **44**, 77–87.

LIU, Q. 2016 Global instability analysis and control of three-dimensional long open cavity flow. PhD thesis, Universidad Politécnica de Madrid.

LIU, Q., GÓMEZ, F. & THEOFILIS, V. 2015 Linear instability analysis of incompressible flow over a cuboid cavity. In *Procedia IUTAM*, vol. 14, pp. 511–518. *IUTAM-ABCM Symposium on Laminar Turbulent Transition*. Elsevier.

MESEGUER, F., DE VICENTE, J., VALERO, E. & THEOFILIS, V. 2014 On linear instability mechanisms in incompressible open cavity flow. *J. Fluid Mech.* **752**, 219–236.

NAYYAR, P., BARAKOS, G. N. & BADCOCK, K. J. 2007 Numerical study of transonic cavity flows using large-eddy and detached-eddy simulation. *Aeronaut. J.* **111** (1117), 153–164.

ÖZSOY, E., RAMBAUD, P., STITOU, A. & RIETHMULLER, M. L. 2005 Vortex characteristics in laminar cavity flow at very low Mach number. *Exp. Fluids* **38**, 133–145.

PEPLINSKI, A., SCHLATTER, P., FISCHER, P. F. & HENNINGSON, D. S. 2014 Stability tools for the spectral-element code nek5000: application to jet-in crossflow. In *Spectral and High Order Methods for Partial Differential Equations – ICOSAHOM 2012*, Lecture Notes in Computational Science and Engineering, vol. 95, pp. 349–359. Springer.

RODRÍGUEZ, D. & THEOFILIS, V. 2011 On the birth of stall cells on airfoils. *Theor. Comput. Fluid Dyn.* **25**, 105–117.

ROSHKO, A. 1955 Some measurements of flow in a rectangular cutout. *NACA TN* 3488.

ROSSITER, J. 1964 Wind-tunnel experiments on the flow over rectangular cavities at subsonic and transonic speeds. *Aero. Res. Counc. R&M* 3438.

ROWLEY, C. W., COLONUIS, T. & BASU, A. J. 2002 On self-sustained oscillations in two-dimensional compressible flow over rectangular cavities. *J. Fluid Mech.* **455**, 315–346.

SAROHIA, V. 1975 Experimental and analytical investigation of oscillations in flows over cavities. PhD thesis, California Institute of Technology.

SAROHIA, V. 1977 Experimental investigation of oscillations on flows over shallow cavities. *AIAA J.* **15**, 984–991.

SUN, Y., NAIR, A. G., TAIRA, K., CATTAFESTA, L. N., UKEILEY, L. S. & BRÉS, G. A. 2014 Numerical simulations of subsonic and transonic open-cavity flows. *AIAA Paper* 2014-3092.

THEOFILIS, V. 2003 Advances in global linear instability analysis of nonparallel and three-dimensional flows. *Prog. Aerosp. Sci.* **39**, 249–315.

THEOFILIS, V. 2011 Global linear instability. *Annu. Rev. Fluid Mech.* **43**, 319–352.

THEOFILIS, V., HEIN, S. & DALLMANN, U. 2000 On the origins of unsteadiness and three-dimensionality in a laminar separation bubble. *Phil. Trans. R. Soc. Lond.* A **358**, 3229–3246.

YAMOUNI, S., SIPP, D. & JACQUIN, L. 2013 Interaction between feedback aeroacoustic and acoustic resonance mechanisms in a cavity flow: a global stability analysis. *J. Fluid Mech.* **717**, 134–165.

YAO, H., COOPER, R. K. & RAGHUNATHAN, S. 2004 Numerical simulation of incompressible laminar flow over three dimensional rectangular cavities. *Trans. ASME J. Fluids Engng* **126**, 919–927.

ZHANG, K. & NAGUIB, A. M. 2008 Effect of cavity width on the unsteady pressure in a low-Mach-number cavity. *AIAA J.* **46**, 1878–1880.

ZHANG, K. & NAGUIB, A. M. 2011 Effect of finite cavity width on flow oscillation in a low-Mach-number cavity. *Exp. Fluids* **51**, 1209–1229.

ZHANG, Y., SUN, Y., ARORA, N., CATTAFESTA, L. N., TAIRA, K. & UKEILEY, L. 2015 Suppression of cavity oscillations via three-dimensonal steady blowing. *AIAA Paper* 2015-3219.